

Article

Halogen Bonding and CO-Ligand Blue-Shift in Hybrid Organic—Organometallic Cocrystals [CpFe(CO)₂X] (C₂I₄) (X = Cl, Br)

Yury Torubae^{1,*} , Ivan Skabitskiy¹, Sergey Shapovalov¹, Olga Tikhonova¹ and Anna Popova²

¹ Kurnakov Institute of General and Inorganic Chemistry, Russian Academy of Sciences, 119991 Moscow, Russia; skabitskiy@gmail.com (I.S.); schss@yandex.ru (S.S.); olga_tikhonova12@mail.ru (O.T.)

² The Faculty of Physics, Mathematics and Natural Sciences, Peoples' Friendship University of Russia (RUDN), 117198 Moscow, Russia; a.popova1701@gmail.com

* Correspondence: torubae@igic.ras.ru

Abstract: This work is focused on the complex interplay of geometry of I ··· X halogen bonds (HaB) and intermolecular interaction energy in two isomorphous cocrystals [CpFe(CO)₂X] (C₂I₄) (X = Cl (1), Br (2)). Their IR-spectroscopic measurements in solid state and solution demonstrate the blue-shift of CO vibration bands, resulting from I ··· X HaB. The reluctance of their iodide congener [CpFe(CO)₂I] to form the expected cocrystal [CpFe(CO)₂I] (C₂I₄) is discussed in terms of different molecular electrostatic potential (MEP) of the surface of iodide ligands, as compared with chloride and bromide, which dictate a different angular geometry of HaB around the metal-I and metal-Br/Cl HaB acceptors. This study also suggests C₂I₄ as a reliable HaB donor cofomer for metal-halide HaB acceptors in the crystal engineering of hybrid metal–organic systems.



Citation: Torubaev, Y.; Skabitskiy, I.; Shapovalov, S.; Tikhonova, O.; Popova, A. Halogen Bonding and CO-Ligand Blue-Shift in Hybrid Organic—Organometallic Cocrystals [CpFe(CO)₂X] (C₂I₄) (X = Cl, Br). *Crystals* **2022**, *12*, 412. <https://doi.org/10.3390/cryst12030412>

Academic Editor: Marta E. G. Mosquera

Received: 26 February 2022

Accepted: 15 March 2022

Published: 17 March 2022

Publisher's Note: MDPI stays neutral with regard to jurisdictional claims in published maps and institutional affiliations.



Copyright: © 2022 by the authors. Licensee MDPI, Basel, Switzerland. This article is an open access article distributed under the terms and conditions of the Creative Commons Attribution (CC BY) license (<https://creativecommons.org/licenses/by/4.0/>).

Keywords: halogen bonding; σ -hole; cocrystal; blue-shift

1. Introduction

Two functional groups in tetrahaloethenes, C₂X₄ (X = F, Cl, Br, I), namely double bonds and halogen, provide at least two possible types of their coordination in transition metal complexes: the π -coordination of C=C double bond and donor–acceptor interaction between the halogen atom and metal centre. Both these types are exemplified by a sufficient number of crystal structures deposited in the Cambridge Structural Database (CSD). Each category has its certain specificity: C=C double bond coordination is known only for rather compact tetrafluoroethene (C₂F₄) with platinum group metals (Pt, Pd, Rh), while I → M donation was found only in tetraiodide C₂I₄ complexes with Ag and Au [1,2]. Recent advances in the investigation of non-covalent interactions and their use in supramolecular design revealed two more types of intermolecular interactions between C₂I₄ and metal complexes: “regular” halogen bonding (HaB) between iodine functions of C₂I₄ and HaB-accepting halide ligands in metal complexes, investigated by the same group [Pt₂I₆] [3], Ni bis(2-oxido-*N,N*-dimethyldiazene-1-carboximidamide) [4] and direct metal-to-iodine donation, or I ··· M halogen bonding (HaB), developed by the group of V. Kukushkin [5]. The former type of “regular” HaB-assisted hybrid metal–organic cocrystals can be considered as a part of a big family of HaB cocrystals between C₂I₄ and halide salt HaB acceptors such as [R₄N]⁺X[−], developed mostly by the efforts of the group of W. Pennington [6]. Unlike the metal-halide supramolecular architectures, such [R₄N]⁺X[−] C₂I₄ salt cocrystals feature more than two (typically four, rarely six) molecules of C₂I₄ in the “coordination sphere” of the halide anion. We were interested in investigating whether such big “coordination numbers” can be achieved in metal-halide cocrystals of C₂I₄. On the other hand, in a continuation of our research of the HaB effect on the electronic structure of transition metal complexes [7], we were interested in the investigation of the crystal and electronic structure of the hybrid

metal–organic cocrystal of transition metal carbonyls and C_2I_4 . Therefore, we cocrystallized $CpFe(CO)_2X$ ($X = Cl, Br, I$) with C_2I_4 and studied the crystal structure, geometry, energy of intermolecular interactions, and IR spectra of the resulting cocrystals.

2. Materials and Methods

2.1. Materials

Solvents were purified, dried, and distilled under an argon atmosphere before use. Commercial C_2I_4 was used without additional purification. The $[CpFe(CO)_2X]$ ($X = Cl, Br, I$) cocrystals were prepared using reported procedures [Brauer].

2.2. General Co-Crystallization Procedure

Cocrystals **1–2** were prepared by the slow evaporation of CH_2Cl_2 solution of cofomers. In a typical experiment, samples of cocrystal **1** suitable for single-crystal XRD investigation were grown in 1.5 mL plastic vial (Eppendorf) containing a solution of $[CpFe(CO)_2X]$ (0.1 mmol) and of C_2I_4 (0.2 mmol) in 0.25 mL of CH_2Cl_2 , which was closed and left at room temperature for 48 h. Red crystals of **1** along with some colorless prisms of C_2I_4 formed. They were washed with 1 mL of hexane, then dried in a stream of argon.

2.3. X-ray Structure Determinations

A Bruker D8 Venture diffractometer (Bruker, Billerica, MA, USA) equipped with graphite-monochromated $Mo\ K\alpha$ radiation (0.71070 Å) was used for the cell determination and intensity data collection for cocrystals **1** and **2** and $CpFe(CO)_2Br$. The data were collected by the standard ϕ - ω scan techniques and were reduced using SAINT v8.37 A (Bruker: Madison, WI, USA). The SADABS (version 2016/2; Bruker, 2016) software was used for scaling and absorption correction. The structures were solved by direct methods and refined by full-matrix least-squares against F^2 using Olex2 and SHELXTL software [8,9]. Non-hydrogen atoms were refined with anisotropic thermal parameters. All hydrogen atoms were geometrically fixed and refined using a riding model.

2.4. Computations

Theoretical calculations were carried out with the ORCA 5.02 program package [10]. A non-hybrid PBE functional [11] dispersion correction with Becke–Johnson damping (D3BJ) [12,13] and a def2-TZVP basis set [14] with small-core pseudopotential for I atoms [15] were used for geometry optimization. Def2/J auxiliary basis [16] was used for Coulomb fitting. Electron density calculations of the resulting geometries were performed using ZORA approximation for scalar relativistic effects [17,18], a hybrid functional PBE0 [19] and an all-electron def2-TZVP basis set reconstructed for ZORA. RIJCOSX approximation [20] in combination with a SARC/J auxiliary basis set [21] was used to improve computational speed. MEP values on $0.002\ e\text{\AA}^{-3}$ isosurfaces were evaluated by the Multiwfn program [22]. MEP figures were prepared using VisMap software [23].

Intermolecular interaction energy calculation and subsequent energy framework generation were performed in Crystal Explorer 17.5 (TONTTO, B3LYP-DGDZVP) for all unique molecular pairs in a molecule's first coordination sphere (4 Å) using experimental crystal geometries.

3. Results

3.1. Preparation and Crystal Structure of $[CpFe(CO)_2X]\cdot(C_2I_4)$ ($X = Cl, Br$)

Cocrystallization of 2:1 C_2I_4 and $CpFe(CO)_2X$ solution in CH_2Cl_2 in the conditions of slow evaporation at room temperature afforded isomorphous 1:1 cocrystals of $[CpFe(CO)_2Cl]\cdot(C_2I_4)$ (**1**) and $[CpFe(CO)_2Br]\cdot(C_2I_4)$ (**2**), respectively. A first glance at their crystal structure reveals the $CpFe(CO)_2X$ molecule connected with four C_2I_4 molecules by $I\cdots X$ HaBs (Figure 1). In turn, each iodine in C_2I_4 molecule forms $I\cdots X$ HaB, so that C_2I_4 molecule is surrounded by four $CpFe(CO)_2X$ molecules (see Figure 2).

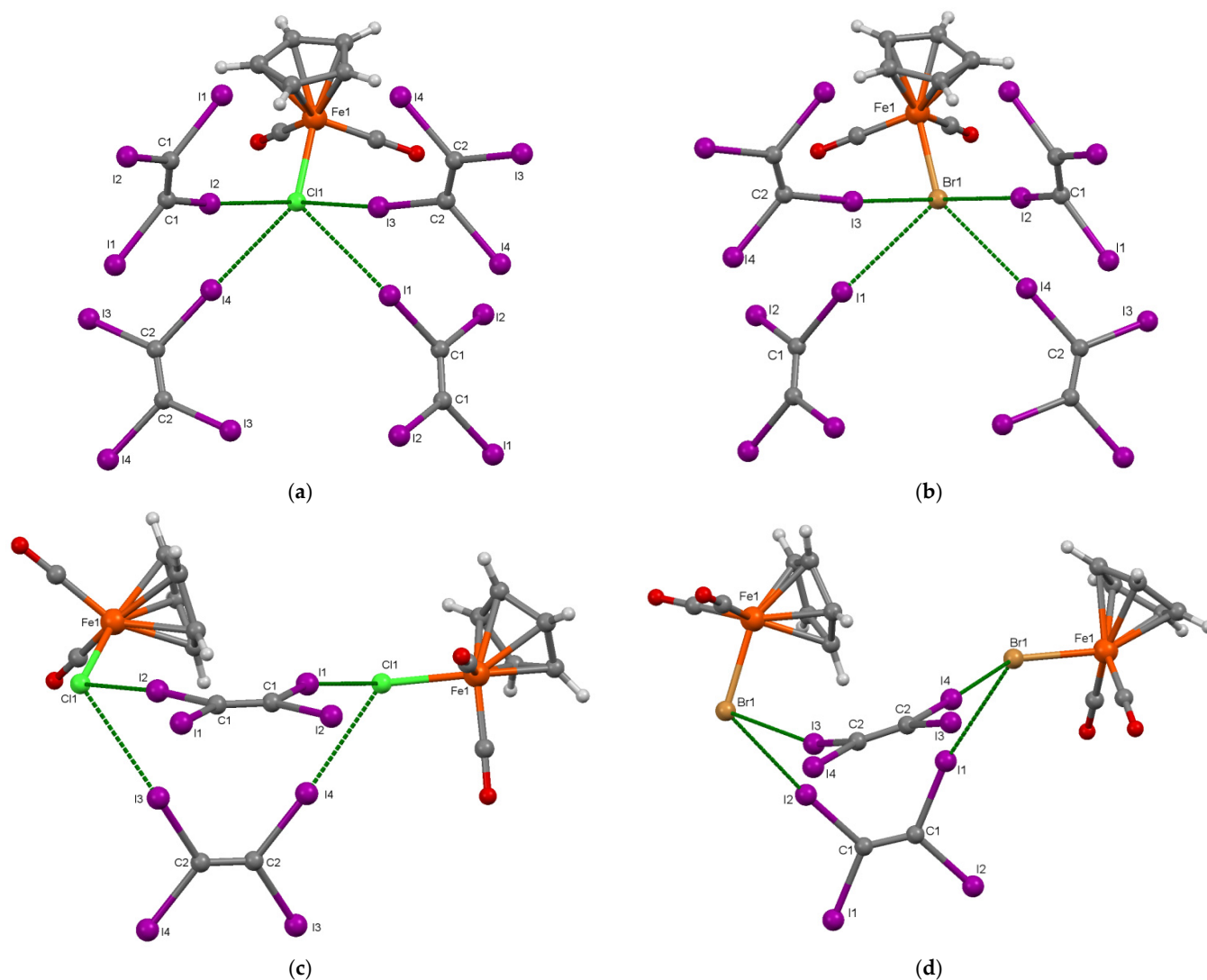


Figure 1. Fragments of the crystal structure of **1** (a,c) and **2** (b,d) showing the HaB-assisted supramolecular arrangement around [CpFe(CO)₂X] molecules (a,b) and two independent C₂I₄ molecules, bridging two [CpFe(CO)₂X] (c,d). Selected interatomic distances in **1** (Å): Fe1–Cl1 2.295(2), Cl1···I1 3.443(2), I3···Cl1 3.382(2), Cl1···I2 3.259(2), Cl1···I4 3.261(2); Selected angles in **1** (°): Fe1–Cl1···I1 114.06(8), Fe1–Cl1···I2 113.40(8), Fe1–Cl1···I3 100.64(8), Fe1–Cl1···I4 130.31(9), C1–I2···Cl1 168.7(3), C1–I1···Cl1 166.4(3), C2–I3···Cl1 162.8(3), C2–I4···Cl1 175.7(3). Selected interatomic distances in **2** (Å): Fe1–Br1 2.430(1), Br1···I1 3.5598(7), Br1···I2 3.3717(7), Br1···I3 3.4517(8), Br1···I4 3.3398(7). Selected angles in **2** (°): Fe1–Br1···I1 112.56(3), Fe1–Br1···I2 112.13(3), Fe1–Br1···I3 97.03(3), Fe1–Br1···I4 134.93(3), C1–I1···Br1 164.3(2), C1–I2···Br1 170.2(2), C2–I3···Br1 161.3(2), C2–I4···Br1 176.0(2).

We can note a slight elongation of the Fe–Br bond in **2** (2.430(1) Å) as compared with 2.4221(4) Å in the native [CpFe(CO)₂Br], and Fe–Cl bond (2.295(2) Å) in **1**, compared with 2.251(7) Å in [CpFe(CO)₂Cl], trapped in a cyclodextrine cage [24].

Tetrahaloethenes C₂I₄ and C₂Br₄ tend to reproduce the layered fragments of their native packing patterns (i.e., in their parent crystal) in their cocrystals such that two of three lattice dimensions of the native C₂X₄ (X = Br, I) and their pyrazine adducts are similar [25–27]. However, close examination of crystal structures **1** and **2** did not reveal any parallels with the crystal structure of the native C₂I₄. The σ -holes at each of four iodine atoms of C₂I₄ in **1** and **2** are directed towards the halide ligands X of CpFe(CO)₂X, forming I···X HaBs (Figure 2); therefore, short I···I interactions (HaBs) between C₂I₄ molecules are absent in these cocrystals. Each halide ligand of CpFe(CO)₂X in turn forms four I···X

HaBs (Figure 1). The lengths of these $I \cdots X$ HaBs vary in the range of 3.259(2) Å–3.443(2) Å in **1** to 3.3398(7) Å–3.5598(7) Å in **2**, but in general, they are shorter than the respective sums of vdW radii, and their Fe-X \cdots I angles suggest that all of these HaBs are genuine (type-II [28]) HaBs.

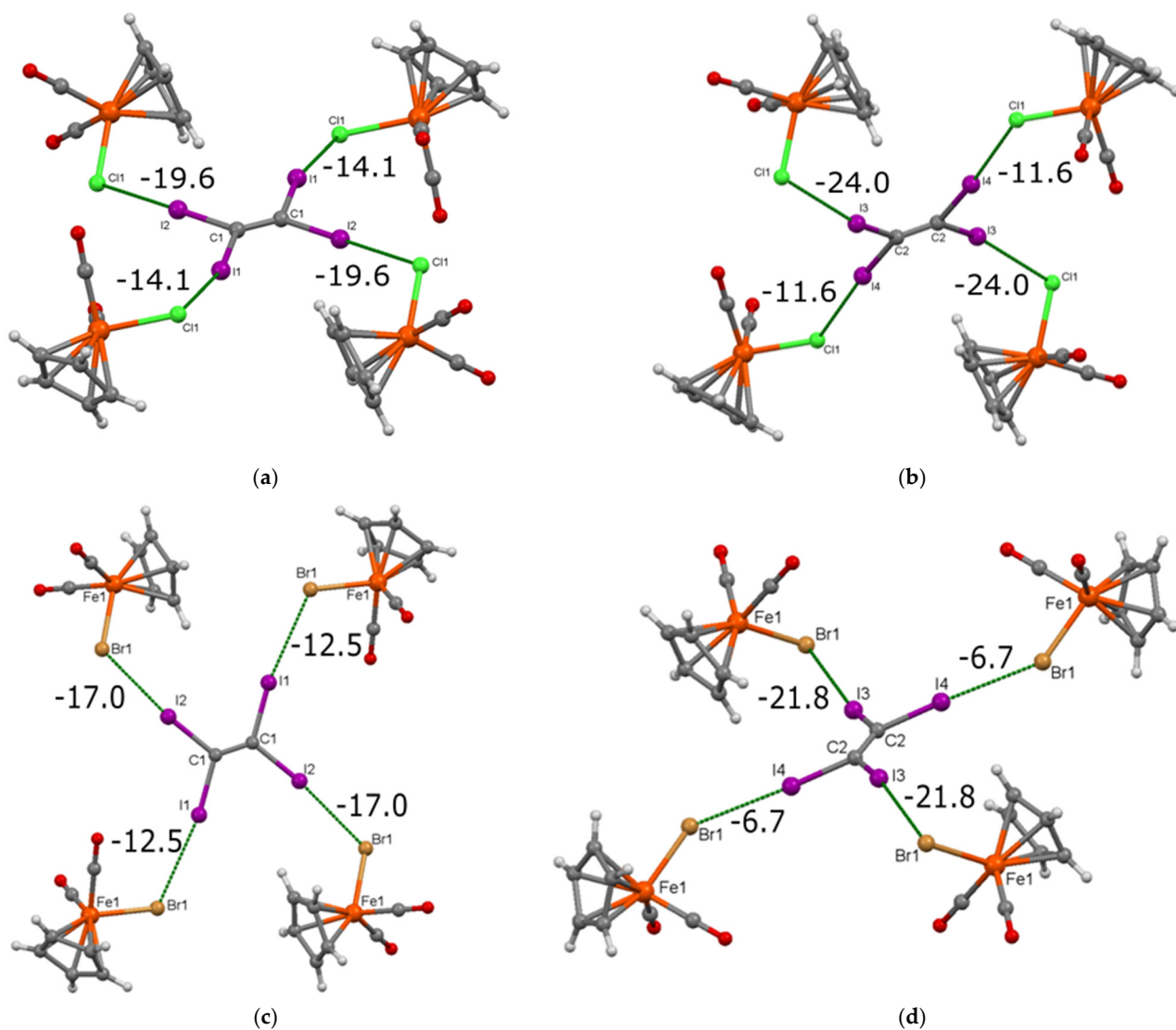


Figure 2. Fragments of the crystal structure of **1**, showing the supramolecular arrangement and intermolecular interaction energies around two independent C₂I₄ molecules in **1** (a,b) and in **2** (c,d). Energy values are indicated in kJ/mol. Note that these are the total intermolecular interaction energies of the given molecular pairs, but not specific $I \cdots X$ HaB energies.

As a final structural remark, we can mention that in the same conditions as for CpFe(CO)₂X (X = Cl, Br), the CpFe(CO)₂I did not afford any cocrystalline product with C₂I₄ and only starting materials were recovered from the reaction mixture. The reluctance of CpFe(CO)₂I in terms of the supramolecular interaction with C₂I₄ is most likely due not to the weak properties of the iodide ligand as an acceptor compared with chloride and bromide, but to its increased demands on the angles at which stable $I \cdots X$ -Fe HaB can form. As we demonstrated earlier [7], in some cases (against the background of a fairly stable and flexible $I \cdots Cl$ -M and $I \cdots Br$ -M HaBs), the formation of $I \cdots I$ -M HaB was not observed precisely because of steric factors—the impossibility of placing a HaB donor in the equatorial plane (of the nucleophilic p-belt) of the iodine ligand due to the sterically crowded environment around it. For the same reason, the HaB-assisted cocrystals

of metal-chloride and metal-bromide HaB donors are usually isomorphous, while metal-I cocrystals with the same HaB donors stay apart [29]. We can assume that since the Fe1-X1...I4 angles in **1** and **2** (130° and 135° , respectively, Figure 1) are clearly above the right angle and 106° – 113° observed before in $[\text{Bu}_4\text{P}][\text{Pt}_2\text{I}_6]$ C_2I_4 cocrystal [3], the same arrangement for $\text{CpFe}(\text{CO})_2\text{I}$ and C_2I_4 is not stable. Furthermore, we can speculate that other arrangements for $\text{CpFe}(\text{CO})_2\text{I}$ and C_2I_4 may not provide sufficient profit in energy and packing as compared with the starting materials. Apart from the higher rigidity of the iodide-centered HaBs and consequent steric problems of achieving the optimal angles, another contribution to the failure of $\text{CpFe}(\text{CO})_2\text{I}$ to form cocrystals with C_2I_4 may come from the lower HaB acceptor properties of the iodide as compared with bromide and chloride. In particular, the series of studies on halopyridinium salts with halide anions as HaB acceptors demonstrated that although the nature of the halide anion provides a secondary effect on the HaB strength, the HaBs with iodide are generally weaker than those with bromide and chloride as HaB acceptors [30–35].

3.2. Electronic Structure and IR Spectroscopy

Molecular electrostatic potential (MEP) mapping of C_2I_4 shows a rather pronounced and equivalent σ -hole on each iodine atom ($V_{\text{max}} = -36.5$ kcal/mol, Figure 3).

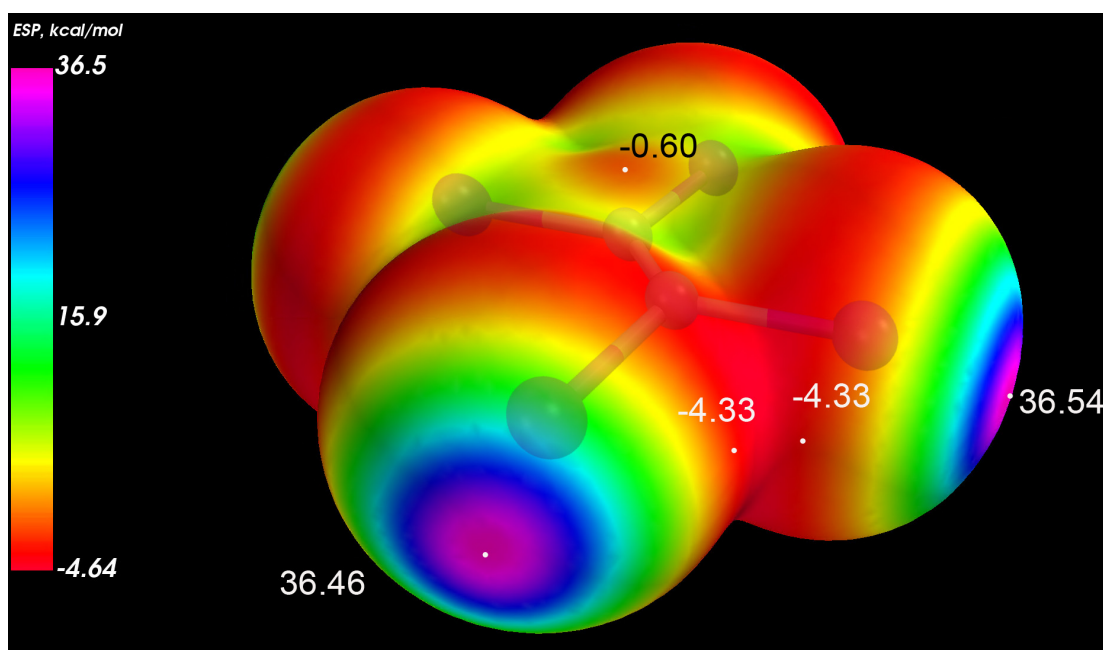


Figure 3. Molecular electrostatic potential (MEP) maps for an isolated molecule of C_2I_4 ($0.002 \text{ e}/\text{\AA}^3$ electron density isosurface).

The σ -holes in C_2I_4 are only 5 kcal less “deep” than in 1,4-diiodotetrafluorobenzene (1,4-DITFB, $V_{\text{max}} = -40.4$ kcal/mol [36]), the classic HaB donor, which was successfully used as a cofomer for $\text{CpFe}(\text{CO})_2\text{X}$ ($\text{X} = \text{Cl}, \text{Br}, \text{I}, \text{TePh}$) in our earlier study [7].

HaB between the positive area of iodine function of C_2I_4 and the nucleophilic area of ligand X in $\text{CpFe}(\text{CO})_2\text{X}$ is sufficient to shift the electron density from the M-X bond and therefore to reduce $\text{M} \rightarrow \text{CO}$ back-donation [37]. The resulting depopulation of the $\pi^*\text{C-O}$ LUMO orbital slightly strengthens the CO bond and consequently shifts its vibrational band to the higher frequency area. This is also in good agreement with the slight elongation of Fe-X bonds in **1** and **2** compared with the free molecules of $[\text{CpFe}(\text{CO})_2\text{X}]$ mentioned in Section 3.1.

The series of $[\text{CpFe}(\text{CO})_2\text{X}]$ (1,4-DITFB) ($\text{X} = \text{Cl}, \text{Br}, \text{I}, \text{TePh}$) cocrystals demonstrated the 5 – 10 cm^{-1} blue shift of CO vibrational bands as compared with the respective parent

$\text{CpFe}(\text{CO})_2\text{X}$. Therefore, the 5–7 cm^{-1} blue shifts of CO vibration bands in the solid-state ATR IR spectra of **1** and **2** (as compared with the parent $\text{CpFe}(\text{CO})_2\text{Cl}$ and $\text{CpFe}(\text{CO})_2\text{Br}$) were quite expected (Figure 4).

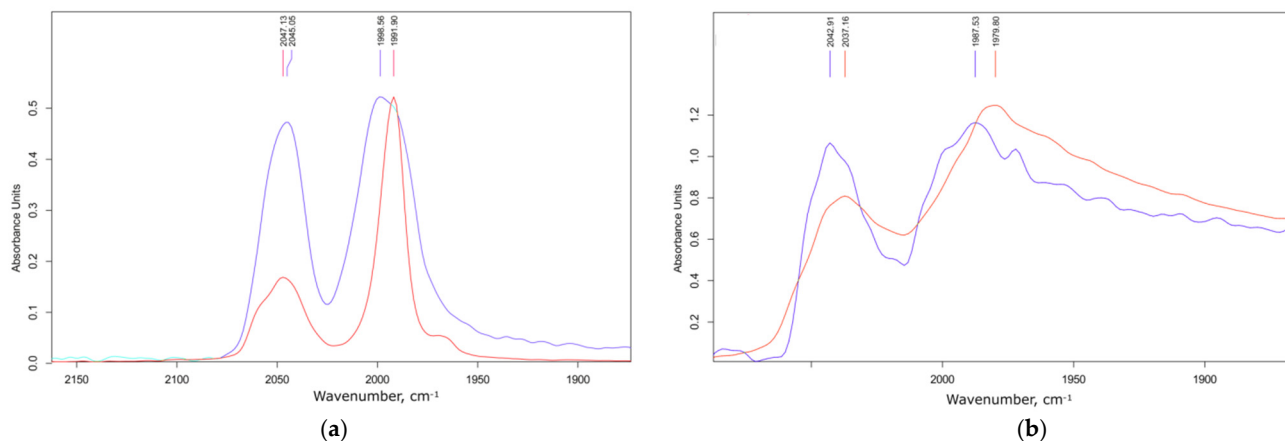


Figure 4. Overlay of the fragments of IR (ATR) spectra of pure $\text{CpFe}(\text{CO})_2\text{Cl}$ (red) and cocrystal **1** (blue, **a**); overlay of $\text{CpFe}(\text{CO})_2\text{Br}$ (red) and **2** (blue, **b**).

Such less pronounced blue shifts of CO groups in **1** and **2** are in good agreement with the longer $\text{I} \cdots \text{Br}$ distances in **2** (3.3398(7)–3.5598(7) Å (Figure 1) as compared with 3.294–3.311 Å in $[\text{CpFe}(\text{CO})_2\text{Br}]$ (1,4-DITFB) [7].

We evaluated the energy of intermolecular interactions between $\text{CpFe}(\text{CO})_2\text{Br}$ and C_2I_4 in **2** (−12.5–−17.0 kJ/mol) and $[\text{CpFe}(\text{CO})_2\text{Br}]$ –1,4-DITFB (−14.6–−15.0 kJ/mol) in the respective cocrystal in Crystal Explorer/TONTO–DGDZVP [38]. These values reflect the total intermolecular interaction energy, but not specific (e.g., HaB) interactions. Intermolecular interactions between C_2I_4 and $\text{CpFe}(\text{CO})_2\text{Br}$ molecules in cocrystal **2** are not limited to $\text{I} \cdots \text{Br}$ HaBs and also include $\text{C-H} \cdots \text{I}$ contacts. The latter may provide a noticeable contribution to the intermolecular adhesion, and therefore the shorter $\text{I} \cdots \text{Br}$ distances (say, $\text{I}2 \cdots \text{Br}1$ 3.3717(7) Å) in combination with the $\text{H}8 \cdots \text{I}2$ contacts (3.1730) correspond to stronger intermolecular bonding (−17 kJ/mol), while the $\text{I} \cdots \text{Br}$ HaB match the longest $\text{I} \cdots \text{Br}$ separation ($\text{I}1 \cdots \text{Br}1$ 3.5598(7) Å) and weaker intermolecular interaction (−12.5 kJ/mol). It should be noted that $\text{I} \cdots \text{Br}$ distances in **2** are the result of a complex interplay of intermolecular interactions and cannot be directly compared with those in $[\text{CpFe}(\text{CO})_2\text{Br}]$ (1,4-DITFB), so we can only generally conclude that the HaB interaction of the bromide ligand in $[\text{CpFe}(\text{CO})_2\text{Br}]$ with four C_2I_4 is comparable to that with two 1,4-DITFBs.

4. Conclusions

C_2I_4 is a reliable HaB donor cofomer for the organometallic halides, particularly for $\text{CpFe}(\text{CO})_2\text{X}$ ($\text{X} = \text{Cl}, \text{Br}$). The strong demand of the iodide ligand to accept the HaB strictly in the equatorial plane results in the reluctance of $\text{CpFe}(\text{CO})_2\text{I}$ to cocrystallize with C_2I_4 . The formation of four $\text{I} \cdots \text{X}$ HaBs around each X ligand results in 5–7 cm^{-1} blue shifts of CO vibration bands in the solid-state ATR IR spectra of $[\text{CpFe}(\text{CO})_2\text{X}] \text{C}_2\text{I}_4$ ($\text{X} = \text{Cl}, \text{Br}$) cocrystals.

Author Contributions: Conceptualization, methodology and manuscript preparation, Y.T. and I.S.; XRD crystallography and QC computations, synthesis and spectroscopic measurements, O.T., A.P. and S.S. All authors have read and agreed to the published version of the manuscript.

Funding: This research was funded by the Ministry of Science and Higher Education of the Russian Federation, grant number 075-15-2020-779.

Data Availability Statement: Atomic coordinates and other structural parameters of **1-x** have been deposited with the Cambridge Crystallographic Data Centre: CCDC 2154590 (1), CCDC 2154589 (2), and CCDC 2154591 [CpFe(CO)₂Br].

Acknowledgments: We thank the reviewers for their valuable comments.

Conflicts of Interest: The authors declare no conflict of interest. The funders had no role in the design of the study; in the collection, analyses, or interpretation of data; in the writing of the manuscript, or in the decision to publish the results.

References

1. Wu, L.P.; Munakata, M.; Kuroda-Sowa, T.; Maekawa, M.; Suenaga, Y.; Kitamori, Y. Silver(I) tetraiodoethylene complexes with twisted olefin moiety. *Inorg. Chim. Acta* **1999**, *290*, 251–255. [CrossRef]
2. Yamamoto, H.M.; Yamaura, J.-I.; Kato, R. Multicomponent Molecular Conductors with Supramolecular Assembly: Iodine-Containing Neutral Molecules as Building Blocks. *J. Am. Chem. Soc.* **1998**, *120*, 5905–5913. [CrossRef]
3. Eliseeva, A.A.; Ivanov, D.M.; Novikov, A.S.; Rozhkov, A.V.; Korniyakov, I.V.; Dubovtsev, A.Y.; Kukushkin, V.Y. Hexaiododiplatinate(II) as a useful supramolecular synthon for halogen bond involving crystal engineering. *Dalton Trans.* **2020**, *49*, 356–367. [CrossRef]
4. Efimenko, Z.M.; Eliseeva, A.A.; Ivanov, D.M.; Galmés, B.; Frontera, A.; Bokach, N.A.; Kukushkin, V.Y. Bifurcated μ -I-(N,O) Halogen Bonding: The Case of (Nitrosoguanidinate)NiII Cocrystals with Iodine(I)-Based σ -Hole Donors. *Cryst. Growth Des.* **2020**, *21*, 588–596. [CrossRef]
5. Eliseeva, A.A.; Ivanov, D.M.; Rozhkov, A.V.; Ananyev, I.V.; Frontera, A.; Kukushkin, V.Y. Bifurcated Halogen Bonding Involving Two Rhodium(I) Centers as an Integrated σ -Hole Acceptor. *JACS Au* **2021**, *1*, 354–361. [CrossRef] [PubMed]
6. Bailey, R.D.; Hook, L.L.; Watson, R.P.; Hanks, T.W.; Pennington, W.T. Tetraiodoethylene: A supramolecular host for Lewis base donors. *Cryst. Eng.* **2000**, *3*, 155–171. [CrossRef]
7. Torubaev, Y.V.; Skabitskiy, I.V.; Rusina, P.; Pasynskii, A.A.; Rai, D.K.; Singh, A. Organometallic halogen bond acceptors: Directionality, hybrid cocrystal precipitation, and blueshifted CO ligand vibrational band. *Cryst. Eng. Comm.* **2018**, *20*, 2258–2266. [CrossRef]
8. Dolomanov, O.V.; Bourhis, L.J.; Gildea, R.J.; Howard, J.A.K.; Puschmann, H. OLEX2: A complete structure solution, refinement and analysis program. *J. Appl. Cryst.* **2009**, *42*, 339–341. [CrossRef]
9. Sheldrick, G.M. Crystal structure refinement with SHELXL. *Acta Crystallogr. Sect. C Struct. Chem.* **2015**, *71*, 3–8. [CrossRef] [PubMed]
10. Neese, F. Software update: The ORCA program system, version 4.0. *WIREs Comput. Mol. Sci.* **2017**, *8*, e1327. [CrossRef]
11. Perdew, J.P.; Burke, K.; Ernzerhof, M. Generalized Gradient Approximation Made Simple. *Phys. Rev. Lett.* **1996**, *77*, 3865–3868, Erratum in *Phys. Rev. Lett.* **1997**, *78*, 1396. [CrossRef] [PubMed]
12. Grimme, S.; Ehrlich, S.; Goerigk, L. Effect of the damping function in dispersion corrected density functional theory. *J. Comput. Chem.* **2011**, *32*, 1456–1465. [CrossRef] [PubMed]
13. Grimme, S.; Antony, J.; Ehrlich, S.; Krieg, H. A consistent and accurate ab initio parametrization of density functional dispersion correction (DFT-D) for the 94 elements H-Pu. *J. Chem. Phys.* **2010**, *132*, 3297. [CrossRef]
14. Weigend, F.; Ahlrichs, R. Balanced basis sets of split valence, triple zeta valence and quadruple zeta valence quality for H to Rn: Design and assessment of accuracy. *Phys. Chem. Chem. Phys.* **2005**, *7*, 3297. [CrossRef] [PubMed]
15. Metz, B.; Stoll, H.; Dolg, M. Small-core multiconfiguration-Dirac–Hartree–Fock-adjusted pseudopotentials for post-d main group elements: Application to PbH and PbO. *J. Chem. Phys.* **2000**, *113*, 2563–2569. [CrossRef]
16. Weigend, F. Accurate Coulomb-fitting basis sets for H to Rn. *Phys. Chem. Chem. Phys.* **2006**, *8*, 1057–1065. [CrossRef]
17. Lenthe, E.v.; Baerends, E.J.; Snijders, J.G. Relativistic regular two-component Hamiltonians. *J. Chem. Phys.* **1993**, *99*, 4597–4610. [CrossRef]
18. van Wüllen, C. Molecular density functional calculations in the regular relativistic approximation: Method, application to coinage metal diatomics, hydrides, fluorides and chlorides, and comparison with first-order relativistic calculations. *J. Chem. Phys.* **1998**, *109*, 392–399. [CrossRef]
19. Adamo, C.; Barone, V. Toward reliable density functional methods without adjustable parameters: The PBE0 model. *J. Chem. Phys.* **1999**, *110*, 6158–6170. [CrossRef]
20. Izsák, R.; Neese, F. An overlap fitted chain of spheres exchange method. *J. Chem. Phys.* **2011**, *135*, 144105. [CrossRef]
21. Pantazis, D.A.; Neese, F. All-Electron Scalar Relativistic Basis Sets for the Lanthanides. *J. Chem. Theory Comput.* **2009**, *5*, 2229–2238. [CrossRef] [PubMed]
22. Lu, T.; Chen, F. Multiwfn: A multifunctional wavefunction analyzer. *J. Comput. Chem.* **2012**, *33*, 580–592. [CrossRef] [PubMed]
23. Anisimov, A. VisMap. Available online: <https://github.com/aaan1s/VisMap> (accessed on 3 December 2021).
24. Balula, S.S.; Coelho, A.C.; Braga, S.S.; Hazell, A.; Valente, A.A.; Pillinger, M.; Seixas, J.D.; Romão, C.C.; Gonçalves, I.S. Influence of Cyclodextrins on Catalytic Olefin Epoxidation with Metal–Carbonyl Compounds. Crystal Structure of the TRIMEB Complex with CpFe(CO)₂Cl. *Organometallics* **2007**, *26*, 6857–6863. [CrossRef]

25. Dahl, T.; Hassel, O. A Close Relationship between the Crystal Structure of an Acceptor and that of in Addition Compound. *Acta Chem. Scand.* **1966**, *20*, 2009. [[CrossRef](#)]
26. Dahl, T.; Hassel, O. Relationship between Crystal Structures of Tetraiodoethylene and its 1:1 Pyrazine Compound. *Acta Chem. Scand.* **1968**, *22*, 715. [[CrossRef](#)]
27. Dahl, T.; Hassel, O. Crystal Structures of Tetrabromoethylene and of Pyrazine 1:1 of Tetrabromo-resp Tetraiodoethylene. *Acta Chem. Scand.* **1968**, *22*, 8. [[CrossRef](#)]
28. Desiraju, G.R.; Parthasarathy, R. The nature of halogen—Halogen interactions: Are short halogen contacts due to specific attractive forces or due to close packing of nonspherical atoms? *J. Am. Chem. Soc.* **1989**, *111*, 8725–8726. [[CrossRef](#)]
29. Torubaev, Y.; Skabitsky, I.; Lyssenko, K.A. Stages of Kitaigorodsky Aufbau Principle Detached in the Cocrystals of Cp₂MX₂ (M = Ti, Zr; X = Cl, Br, I) with σ - and π -Hole Donors. *Cryst. Growth Des.* **2021**, *22*, 1244–1252. [[CrossRef](#)]
30. Awwadi, F.F.; Willett, R.D.; Peterson, K.A.; Twamley, B. The Nature of Halogen-Halide Synthons: Theoretical and Crystallographic Studies. *J. Phys. Chem. A* **2007**, *111*, 2319–2328. [[CrossRef](#)]
31. Freytag, M.; Jones, P.G.; Ahrens, B.; Fischer, A.K. Hydrogen bonding and halogen–halogen interactions in 4-halopyridinium halides. *New J. Chem.* **1999**, *23*, 1137–1139. [[CrossRef](#)]
32. Frey, M.; Jones, P.G. Secondary Bonding Interactions in Some Halopyridinium and Dihalopyridinium Halides. *Z. Für Nat. B* **2001**, *56*, 889–896. [[CrossRef](#)]
33. Fotović, L.; Stilinović, V. Halogenide anions as halogen and hydrogen bond acceptors in iodopyridinium halogenides. *Cryst. Eng. Comm.* **2020**, *22*, 4039–4046. [[CrossRef](#)]
34. Fotović, L.; Bedeković, N.; Stilinović, V. Evaluation of Halogenopyridinium Cations as Halogen Bond Donors. *Cryst. Growth Des.* **2021**, *21*, 6889–6901. [[CrossRef](#)]
35. Fotović, L.; Bedeković, N.; Stilinović, V. Isostructural Halogen Exchange and Halogen Bonds: The Case of N-(4-Halogenobenzyl)-3-halogenopyridinium Halogenides. *Cryst. Growth Des.* **2022**, *22*, 1333–1344. [[CrossRef](#)] [[PubMed](#)]
36. Aakeröy, C.B.; Baldrighi, M.; Desper, J.; Metrangolo, P.; Resnati, G. Supramolecular Hierarchy among Halogen-Bond Donors. *Chem. Eur. J.* **2013**, *19*, 16240–16247. [[CrossRef](#)] [[PubMed](#)]
37. Bistoni, G.; Rampino, S.; Scafuri, N.; Ciancaleoni, G.; Zuccaccia, D.; Belpassi, L.; Tarantelli, F. How pi back-donation quantitatively controls the CO stretching response in classical and non-classical metal carbonyl complexes. *Chem. Sci.* **2016**, *7*, 1174–1184. [[CrossRef](#)] [[PubMed](#)]
38. Spackman, P.R.; Turner, M.J.; McKinnon, J.J.; Wolff, S.K.; Grimwood, D.J.; Jayatilaka, D.; Spackman, M.A. CrystalExplorer: A program for Hirshfeld surface analysis, visualization and quantitative analysis of molecular crystals. *J. Appl. Crystallogr.* **2021**, *54*, 1006–1011. [[CrossRef](#)] [[PubMed](#)]